Mem. S.A.It. Vol. 92, 27

**Memorie** della


# Stellar compact-object binaries in the era of gravitational-wave Astronomy

N. Giacobbo[1,2,3]

[1] Dipartimento di Fisica e Astronomia "G. Galilei" – Università degli Studi di Padova, vicolo dell'Osservatorio 3, I-35122, Padova, Italy
[2] INAF – Istituto Nazionale di Astrofisica – Osservatorio Astronomico di Padova, vicolo dell'Osservatorio 5, I-35122, Padova, Italy
[3] INFN – Istituto Nazionale di Fisica Nucleare – Sezione di Padova, via Marzolo 8, I-35131, Padova, Italy
e-mail: giacobbo.nicola@gmail.com

**Abstract.** During my PhD, I studied the demography of compact-object binaries in different environments through population-synthesis simulations. The main goal is to better understand the evolutionary pathways of compact-object binaries and their dependence on the properties of stellar progenitors (e.g. metallicity). First of all, I developed MOBSE (an acronym for 'Massive Objects in Binary Stellar Evolution'), a custom version of the binary population-synthesis code BSE, that includes the most recent stellar wind models. Then, I used this tool to explore the impact of metallicity on the formation of merging compact-object binaries, finding that the progenitor's metallicity is crucial in determining the mass of the resulting black hole. I have also studied the critical common-envelope phase and the effect of supernova kicks on binary demography. From my simulations emerges that the efficiency of ejecting the common envelope has a strong impact on the formation of compact-object binaries able to merge within a Hubble time. Moreover, I proposed a new treatment for the natal kicks in population-synthesis codes that matches the proper motion of Galactic pulsars and naturally accounts for the differences between the different flavour of supernova explosions.

**Key words.** Stars: black holes – Stars: neutron stars – Methods: numerical – Gravitational waves – Binary: general

## 1. Introduction

On 14th September 2015, about a hundred years after the formulation of general relativity by Albert Einstein, the LIGO-Virgo collaboration (LVC) observed for the very first time a gravitational-wave signal (Abbott et al., 2016). GW150914, the first event, was interpreted as the merger of two black holes (BHs) and marks the dawn of a new era for astronomy and fundamental physics. Other ten GW detections were reported by the LVC during the first two observational runs (Abbott et al., 2019a): nine additional binary black holes (BBHs; Abbott et al. 2019b) and a binary neutron star (BNS) merger (Abbott et al., 2017). The first half of the third LIGO–Virgo observing run has resulted in 39 new detections (Abbott et al., 2020a), and we expect many more observa-

tions in the years to come. These observations open completely new perspectives on the study of compact-object binaries (COBs) and pose a fundamental question: what are the astrophysical formation channels of merging COBs?

Some recent studies seem to suggest that the vast majority of massive stars are born in binaries (Sana et al., 2012; Moe & Di Stefano, 2017). That makes the evolution of massive stars in isolated binaries[1] one of the most promising channels to understand the formation of COBs. My Thesis aims to investigate the formation of COBs through the evolution of isolated massive binaries. In particular, I studied the main evolutionary pathways of COBs (e.g., common envelope) and their dependence on the properties of progenitor stars (e.g., stellar metallicity and mass).

The next sections are organised as follows. In section 2, I introduce MOBSE, the population-synthesis code I developed and used for my studies. In section 3, there is a summary of the setups of my simulations. Then, I discuss the effect of metallicity (section 4), the importance of the common envelope (section 5) and the impact of natal kicks (section 6) on the formation of merging COBs. Finally, I present the merger rate density obtained from my simulations section 7, and in section 8, there is a summary of the work.

## 2. MOBSE: a new tool

Population-synthesis codes represent a powerful tool for studying the formation and evolution of massive binaries. Indeed, by combining single stellar evolution (including the mechanism of supernova explosion) with binary-evolution processes (e.g. common envelope, tidal interaction, mass transfers), binary population-synthesis codes enable the rapid simulation of a large number of binary systems. That makes binary population-synthesis codes the perfect means to study, from a statistical point of view, the properties

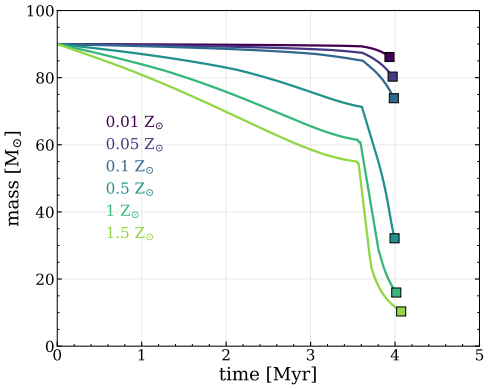


**Fig. 1.** Mass evolution of a star with $M_{\rm ZAMS}$ $M_\odot$ evolved with MOBSE. Different color represent the mass evolution assuming different values for the metallicity $Z \in [0.01, 0.05, 0.1, 0.5, 1, 1.5]$ $Z_\odot$. The squares identify the mass of the star at the of the carbon burning.

of binary populations as well as the rate of occurrence of specific astrophysical events (e.g. merger of COBs).

During my PhD, I developed the code MOBSE[2] ('Massive Objects in Binary Stellar Evolution', see Giacobbo et al. 2018), which is an upgraded version of the widely used population-synthesis code BSE (Hurley et al., 2002). With respect to BSE, MOBSE contains many novelties mainly related to the evolution of massive stars. Indeed, MOBSE includes an up-to-date model for stellar winds. In particular, MOBSE is one of the few population-synthesis codes that accounts for the dependence of stellar winds on both metallicity $Z$ (Vink et al., 2001; Vink & de Koter, 2005) and the electron-scattering Eddington factor[3] $\Gamma_{\rm e}$ (Gräfener & Hamann, 2008; Gräfener et al., 2011), as described by the following relation (Chen et al., 2015):

[1] Binaries that are gravitationally bound since their birth.

[2] `https://mobse-webpage.netlify.app/about/`

[3] $\Gamma_{\rm e} = L_*/L_{\rm Edd}$, where $L_*$ is the stellar luminosity and $L_{\rm Edd}$ is its Eddington limit.

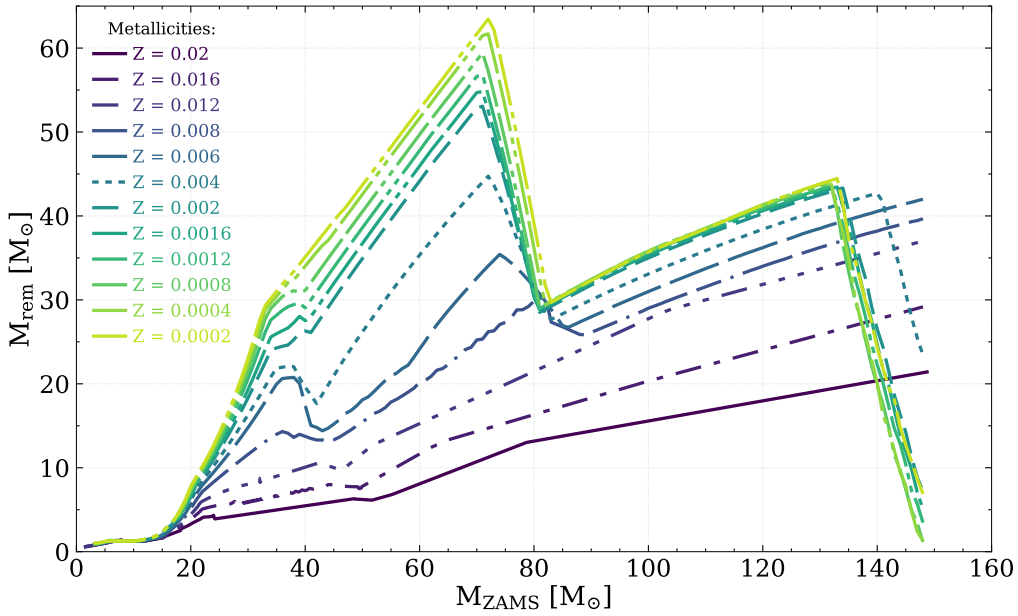


**Fig. 2.** Mass spectrum of compact objects ($M_{\rm rem}$) as a function of the zero age main sequence mass ($M_{\rm ZAMS}$) for different metallicities (Giacobbo & Mapelli, 2018).

$$\dot{M} \propto Z^{\beta}, \tag{1}$$

with

$$\beta = \begin{cases} 0.85 & \text{if } \Gamma_e < 2/3 \\ 2.45 - 2.4\Gamma_e & \text{if } 2/3 \leq \Gamma_e < 1 \\ 0.05 & \text{if } \Gamma_e \geq 1. \end{cases}$$

Thanks to this simple formula, it is possible to account for the fact that stellar winds tend to become insensitive to metallicity when the star is close to be radiation pressure dominated. Figure 1 shows the mass evolution of a star with a zero-age main sequence (ZAMS) mass $M_{\rm ZAMS} = 90\,{\rm M}_\odot$ as obtained with MOBSE and considering six different metallicities ($Z \in [0.01, 0.05, 0.1, 0.5, 1, 1.5]\,{\rm Z}_\odot$, where we assume $\rm Z_\odot = 0.02$). At high metallicity ($Z \gtrsim {\rm Z}_\odot$) the star loses more than 3/4 of its initial mass during its life. In contrast, at low metallicity, the star retains most of its initial mass. It is expected that the final stellar mass, just before the SN, strongly affects the outcome of the SN explosion (Fryer, 1999; Mapelli et al., 2009; Fryer et al., 2012; Langer, 2012). Therefore, stellar winds are crucial to study the compact object because they are the primary cause of the mass loss of a star.

I included in MOBSE new prescriptions to describe the outcomes of supernova (SN) explosions (the *rapid* and *delayed* models presented in Fryer et al. 2012). Those prescriptions assume that the mass of the resulting compact object depends on the mass of carbon-oxygen core and the total final mass pre-SN explosion. Moreover, MOBSE accounts for the treatment of pair-instability and pulsational pair-instability SNe (Spera & Mapelli 2017).

Thanks to MOBSE, I found that the maximum BH mass can be as high as $65{\rm M}_\odot$, significantly larger than previously thought ($\sim 40-50\,{\rm M}_\odot$, Belczynski et al. 2016; Woosley 2017, 2019). In particular, figure 2 shows the mass spectrum of compact remnants as a function of the ZAMS mass of the progenitor stars obtained with MOBSE and assuming different metallicities. On the one hand, figure 2 shows that there is a clear dependence on the metallicity for stars with $M \gtrsim 20\,{\rm M}_\odot$, which indicates the importance of stellar winds. In general, at

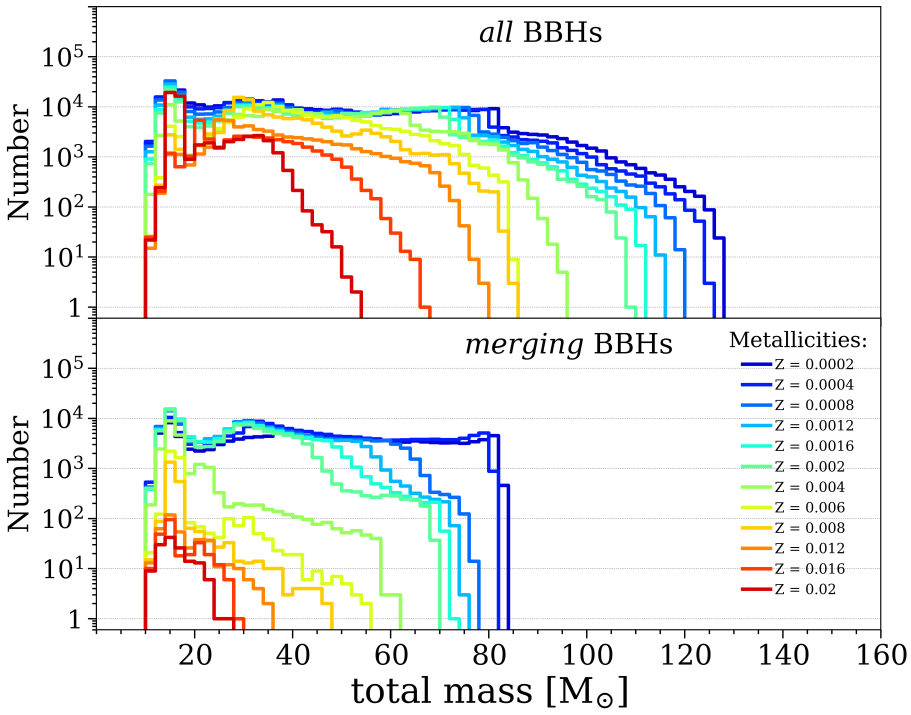


**Fig. 3.** Distributions of the total mass ($m_1 + m_2$) of BBHs that form from a population of $10^8$ massive binary stars, simulated with MOBSE. Upper panel: distributions of all simulated BBHs. Lower panel: distributions of BBHs merging within a Hubble time. Different colours represent different progenitor metallicities, ranging from $Z = 0.0002$ to 0.02 (Giacobbo & Mapelli, 2018).

lower metallicity, the mass of the BHs is higher (Mapelli et al., 2009; Belczynski et al., 2010; Spera et al., 2015; Spera & Mapelli, 2017). On the other hand, for intermediate stars the mass of the resulting compact remnant is affected mostly by the SN engine model rather than progenitor's metallicity (Fryer et al., 2012).

Finally, I implemented in MOBSE i) updated fitting formulas for the core radius (Hall & Tout, 2014); ii) an extension of the mass range to include stars up to 150 $M_\odot$; iii) a different treatment for the Hertzsprung gap donors (HG).

## 3. Simulations setup

With MOBSE I simulated large grids of massive binary stars ($\sim 10^8$ systems per set of simulations) to explore the effect of progenitor metallicity, natal kicks and common envelope on the formation of COBs. I considered initial conditions for the binary properties based on observational constraints. In particular, I sampled the primary masses from a Kroupa initial mass function (Kroupa, 2001) while the masses of the companions are derived from the mass ratio $q = m_2/m_1$ drawn from the distribution proposed by Sana et al. (2012): $\mathcal{F}(q) \propto q^{-0.1}$ with $q \in [0.1 - 1]$. To sample the eccentricity $e$ and the orbital period $P$ I adopted the distributions suggested by Sana et al. (2012): $\mathcal{F}(e) \propto e^{-0.42}$ with $0 \leq e < 1$, $\mathcal{F}(\Pi) \propto \Pi^{-0.55}$ with $\Pi = \log(P/\mathrm{day}) \in [0.15 - 5.5]$, for $e$ and $P$ respectively. Finally, for each set of simulations I considered 12 different metallicities ranging from $Z = 0.0002$ to 0.02.

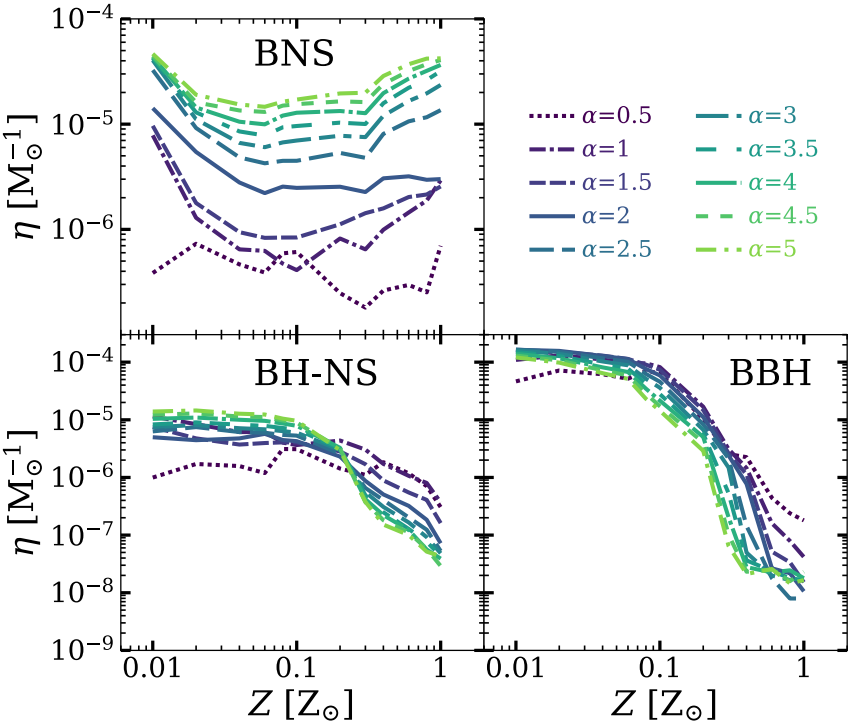


**Fig. 4.** Merger efficiency ($\eta$) as a function of stellar metallicity ($Z$). Different colours represent different values for the common-envelope efficiency $\alpha \in [0.5 - 5]$.

## 4. Effect of metallicity

As discussed in section 2, the mass of BHs is very sensitive to progenitor's metallicity: the lower the metallicity is, the heavier the maximum mass of the remnant. As a consequence, also the total mass of BBHs (i.e. the mass of the primary plus the mass of the secondary BH, $m_1 + m_2$) is strongly affected by progenitor's metallicity. Most importantly, figure 3 shows that the most massive BBHs in my simulations have a total mass $\sim$ 130 $M_\odot$ but do not merge within a Hubble time. In contrast, the most massive BBH mergers from my simulations have a total mass of $\sim$ 90 $M_\odot$. Such difference between the maximum mass of a BBH and that of a BBH that merges within a Hubble time is an effect of mass transfer and common envelope. Indeed, massive stellar progenitor might develop large radii during the supergiant phase. If the initial separation is relatively small, the massive progenitor stars either merge before becoming BHs, or undergo non-conservative mass transfer episodes leading strong mass loss and forming two lighter BHs. In contrast, massive binary stars with large initial orbital separation ($\geq 10^4$ $R_\odot$) do not undergo mass transfer and can lead to the formation of very massive BBHs ($\sim$ 130 $M_\odot$), but the final orbital separation is too large for them to merge.

From these simulations, it is also apparent that the number of mergers depends on metallicity. I defined the merger efficiency as the total numbers of mergers that occur within a Hubble time in a coeval population divided by the total mass of that population ($\eta \propto N_{\rm mergers}/M_{\rm tot}$). Figure 4 shows the behaviour of $\eta$ as a function of metallicity. From figure 4 it is also evident that a population of metal-poor binaries tends to produce more merging BBHs and merging BH-neutron star binaries

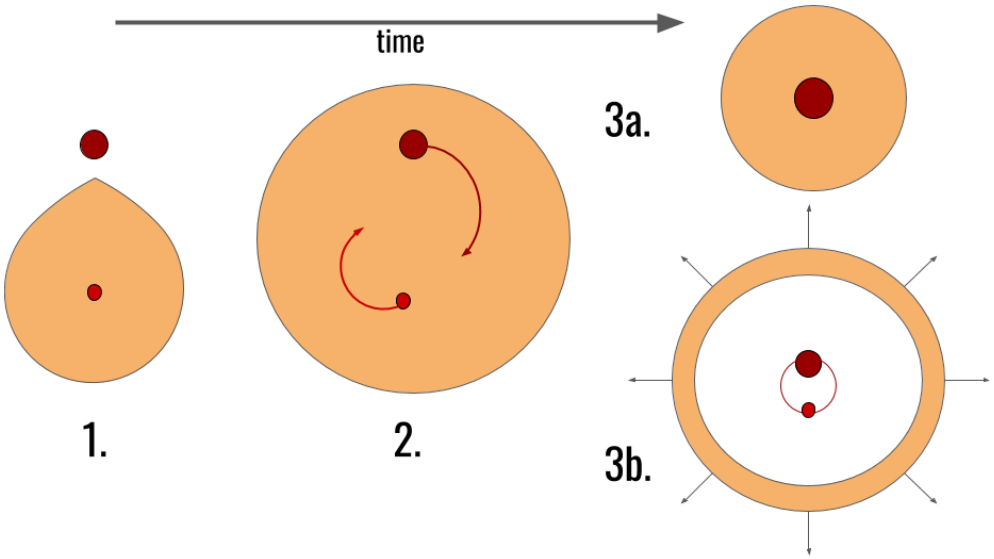


**Fig. 5.** The key stages of the common-envelope evolution of a system composed of an evolved donor star and compact companion. 1): the evolved star fills its Roche lobe; 2): the companion is engulfed. The two core spiral in inside the common envelope until 3a) the envelope is ejected or 3b) the two component merge.

(BHNSs) than a metal-rich population. In particular, for BBHs (BHNSs) the merger efficiency $\eta$ is about four (two) order of magnitude higher at low metallicity ($Z \sim 0.01 Z_{\odot}$) than at solar metallicity ($Z = 0.02$). In contrast, the merger efficiency of BNSs is only mildly affected by progenitor's metallicity.

## 5. Impact of common envelope

In binary systems is not rare that the two stars exchange material between each other. In particular, if the binary is sufficiently close, one of the stellar components might overfill its Roche lobe[4] starting to transfer material to the companion. When this process, named Roche lobe overflow, occurs in an unstable way (e.g. when the stellar radius increases faster than the Roche lobe) or both the stars simultaneously overfill their Roche lobe, the system is expected to either i) enter a common-envelope phase, when the donor shows a clear steep density gradient between the core and the envelope, or ii) merge if there is not a clear distinction between core and envelope.

Thus, the common-envelope evolution starts when two cores are embedded by the same large envelope. Because of the drag generated by the surrounding envelope, the two cores start to spiral-in. During this phase, part of the orbital energy of the cores is transferred to the envelope and transformed into kinetic energy that tends to unbind the envelope. If this energy is sufficient to completely expel the common envelope, then the binary survives and, the result will be a tighter system composed of two naked stellar cores. On the contrary, if the energy released during the spiral-in phase is not enough, the two cores merge during the common-envelope phase. Figure 5 shows a schematic evolution of a

[4] The Roche lobe of a star in a binary systems is the region around the star where orbital material is gravitationally bound to that star. The limit of that region is represented by the innermost equipotential surface that enclose both the components of the system.

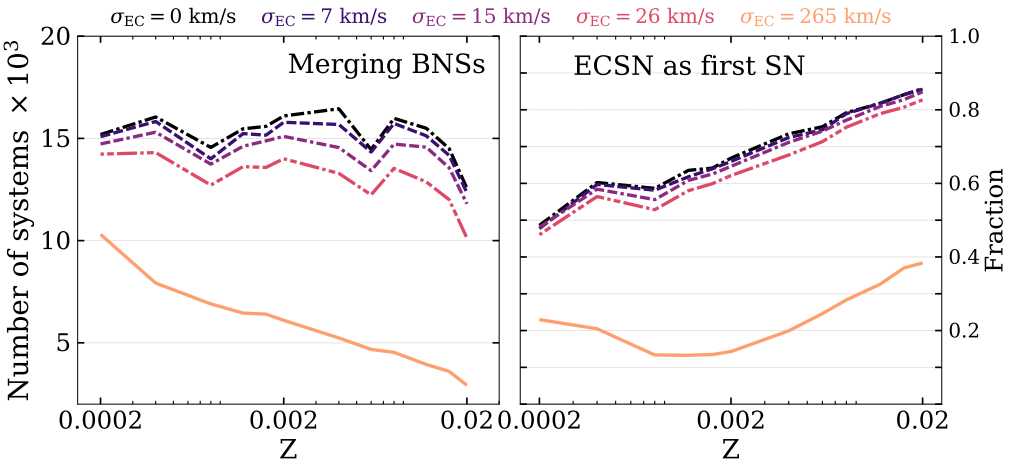


**Fig. 6.** Merging BNSs obtain adopting different $\sigma_{EC} = 0, 7, 15, 26, 265$ km s$^{-1}$. Left-hand panel: number of merging BNSs as a function of progenitor's metallicity. Right-hand panel: fraction of merging BNSs in which the first SN is an electron-capture SN as a function of progenitor's metallicity.

binary systems passing through a common-envelope phase and the possible outcomes.

The common envelope is possibly the most enigmatic binary evolution process. In MOBSE the treatment of common-envelope evolution follows the so-called $\alpha\lambda-$energy formalism (Webbink, 1984; Iben & Livio, 1993; Ivanova et al., 2013). The basic idea is that the energy required to remove the envelope comes entirely from the dissipation of the orbital energy of the binary. Therefore, the outcome of a common-envelope phase depends on both the initial orbital energy of the two cores and the initial binding energy of the envelope. As the name suggests, this formalism relies on two parameters. The first free parameter $\alpha$ represents the fraction of orbital energy available to eject the envelope:

$$\alpha\Delta E_{\rm orb} = \alpha\frac{GM_{c1}M_{c2}}{2}\left(\frac{1}{a_{\rm f}} - \frac{1}{a_{\rm i}}\right), \qquad (2)$$

where $m_{\rm c,1}$ and $m_{\rm c,2}$ are the masses of the two cores and $a_{\rm i}$ and $a_{\rm f}$ are the initial and final orbital separation, respectively. According to equation 2, values of $\alpha$ larger than the unity are un-physical, unless other sources of energy are considered (e.g. recombination energy, enthalpy or nuclear burning from accreted material during the spiral-in phase, see Ivanova et al. 2013). The second free parameter $\lambda$ is introduced to account for the different stellar structure in the calculation of the binding energy of the envelope

$$E_{\rm bin} = \frac{G}{\lambda}\left(\frac{m_{\rm env,1}m_1}{R_1} + \frac{m_{\rm env,2}m_2}{R_2}\right), \qquad (3)$$

where $m_1$ and $m_2$ are the masses of the two stars, $m_{\rm env,1}$ and $m_{\rm env,2}$ are the masses of the stellar envelopes, $R_1$ and $R_2$ are the stellar radii of the two components of the binary. Then, imposing $E_{\rm bin} = \alpha\Delta E_{\rm orb}$ it is possible to derive the final orbital separation $a_{\rm f}$ for which the common envelope is completely ejected. If the sum of the core radii is smaller than $a_{\rm f}$ the system survives the common envelope otherwise, it means that the two cores merge during the common-envelope phase.

My simulations show that common envelope is a crucial process for the formation of merging COBs (Giacobbo & Mapelli, 2018). Indeed, the common-envelope phase helps to shrink the orbital separation of a binary system, facilitating the merger of the final COB. On the other hand, if common envelope is to

efficient in shrinking the orbit (corresponding to a low value of $\alpha$) the binary will not survive the common envelope (e.i. the two members of the binary merge before becoming two compact objects). I found that $\alpha$ has a strong impact on the merger efficiency (see Figure 4). In particular, the higher the $\alpha$ parameter, the higher the merger efficiency of BNSs. Instead, for both BBHs and BHNSs the dependence on $\alpha$ is more complicated because stellar radii of their progenitor stars are strongly affected by metallicity.

## 6. The key role of the natal kicks

It is thought that compact objects receive a kick at birth (natal kick), as a consequence of the SN explosion that are not perfectly symmetric (Janka & Mueller, 1994; Burrows & Hayes, 1996) and anisotropically emit neutrinos Woosley et al. (1987); Fryer & Kusenko (2006); Kusenko et al. (2008); Nagakura et al. (2019). The evolution of COBs is strongly affected by the natal kicks. When the natal kick is high (hundreds of km $s^{-1}$), it will easily disrupt the binary; viceversa, if the kick is small, it does not disrupt the system and may increase its eccentricity, leading to a shorter merger time. In particular, natal kicks have a strong impact on the evolution of BNSs: low natal kicks heavily boost the formation of BNSs (Giacobbo & Mapelli, 2019).

Since it is expected that electron-capture SNe (ECSNe) produce weaker kicks than core-collapse SNe (Dessart et al., 2006; Jones et al., 2013; Schwab et al., 2015; Gessner & Janka, 2018), I explored the impact of the ECSNe on the formation of BNSs (Giacobbo & Mapelli, 2019). In particular, I consider different Maxwellian velocity distributions (with root-mean-square $\sigma_{\rm EC} = 0, 7, 15, 26, 265$ km $s^{-1}$) from which to sample the kicks generated by ECSNe. The left panel of figure 6 shows that the number of merging BNSs scales inversely with $\sigma_{\rm EC}$. In most simulations, I found that more than 50% of the progenitors of BNS mergers undergo at least one ECSN, which is usually the first SN to occur in the binary system (see the right panel in figure 6). My study also confirmed that the binary evolution processes broaden the mass range of stars undergoing an ECSN.

Most population synthesis simulations predict a local BNS merger rate which is below the 90% credible interval inferred from LIGO–Virgo data, unless very low natal kicks are assumed (following a Maxwellian distribution with one-dimensional root-mean square $\sigma < 50$ km $s^{-1}$). However, these low-kick models are not supported by the observations of the proper motions of Galactic young pulsars (Hobbs et al., 2005).

To address this issue, I developed a new formalism for natal kicks (Giacobbo & Mapelli, 2020). The basic idea is that the strength of the natal kick ($v_{\rm kick}$) depends on both the mass ejected during the SN explosion ($m_{\rm ej}$), as suggested by recent hydrodynamical studies (Janka, 2017), and the mass of the compact object ($m_{\rm rem}$), for the conservation of the linear momentum,

$$v_{\rm kick} \propto m_{\rm ej} m_{\rm rem}^{-1}. \quad (4)$$

This formalism has the advantage of naturally accounting for the differences between various types of SNe (e.g. electron-capture SNe, core-collapse SNe and ultra-stripped SNe; Giacobbo & Mapelli 2020). In figure 7, I compare the distributions of natal kicks for neutron stars obtained using different prescriptions: low kicks ($\sigma$15), my new model (EJ1) and the observations of young Galactic pulsars (H05; Hobbs et al. 2005). From figure 7 emerges that, on the one hand binary evolution enhances the number of NSs that receive small kicks, because of dissipative mass transfers that reduce the reservoir of material that can be ejected during the SN explosions. On the other hand, binary evolution also triggers the formation of few NSs with even larger kicks than in the case of single stellar evolution. For the same reason, binary evolution has a smaller impact on NS kicks in models H05 and $\sigma$15 that by construction do not depend significantly on $m_{\rm ej}$.

Compared to the other prescriptions currently adopted by population-synthesis codes, this new approach allows to match both the natal kick distribution of young Galactic pulsars (Hobbs et al., 2005) and the local merger rate

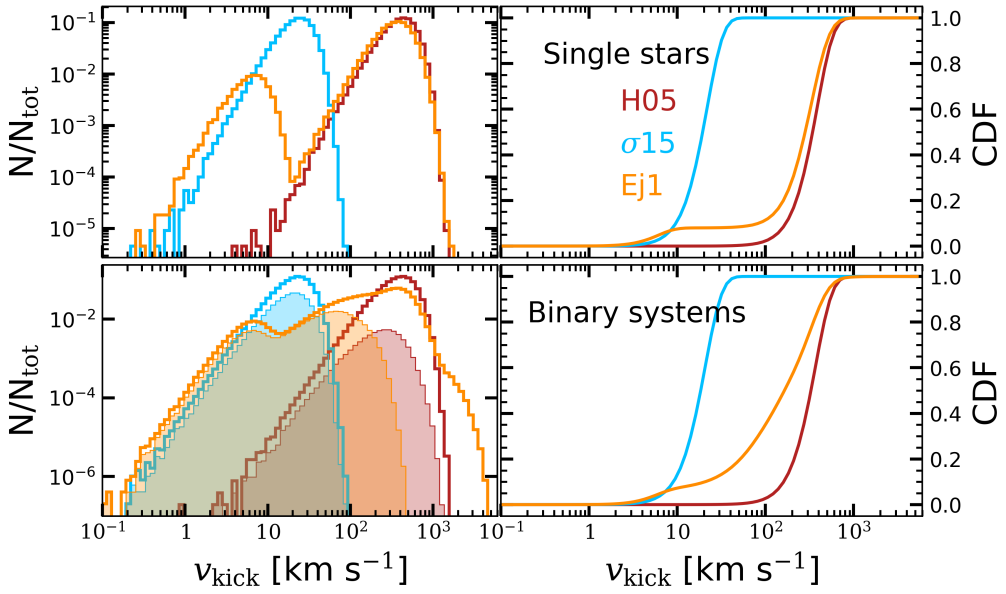


**Fig. 7.** Left-hand panel: distribution of natal kicks for all neutron stars formed from single stars (top) and for those formed from binary systems (bottom). Orange lines: my new model (Ej); red lines: natal kick of young Galactic pulsars based on Hobbs et al. 2005; blue lines: standard model for low kicks sampled from a Maxwellian distribution with root-mean-square equal to 15 km s$^{-1}$ ($\sigma$15). The filled histograms represent the subset of neutron stars that are still gravitationally bound to their companion after the SNe. Right-hand panels: cumulative distributions (CDF) of natal kicks for all NSs (Giacobbo & Mapelli, 2020).

inferred by the LVC (250 – 2810 Gpc$^{-3}$ yr$^{-1}$, Abbott et al. 2020b). Still, to match the LVC merger rate I had to adopt a high common-envelope efficiency (measured by the parameter $\alpha > 3$, see Figure 8).

## 7. Merger rate density

Finally, I developed a semi-analytic method to estimate the local merger rate density of COBs by coupling the results of population-synthesis simulations with prescriptions for the cosmological metallicity evolution (e.g., De Cia et al. 2018) and the star formation rate density evolution (e.g., Madau & Fragos 2017). With this method, I estimated a BHNS local merger rate density of up to few tens of mergers Gpc$^{-3}$ yr$^{-1}$, consistent with the upper limit inferred from the LVC (< 610 Gpc$^{-3}$ yr$^{-1}$ Abbott et al. 2019a). Moreover, I found that the local merger rate density of both BHNSs and BBHs is extremely sensitive to the cosmic metallicity evolution (Giacobbo & Mapelli, 2018).

Adopting my model for natal kicks, I found a local merger rate for BNSs $\sim 400-600$ Gpc$^{-3}$ yr$^{-1}$, consistent with the one inferred from the LVC (250 – 2810 Gpc$^{-3}$ yr$^{-1}$ Abbott et al. 2020b). Figure 8 shows the local merger rate density for different flavours of COBs and different assumptions for the common envelope efficiency $\alpha$. I found that the merger rate density of BNSs is extremely sensitive to the value of $\alpha$: higher value of $\alpha$ leads to higher merger rate density. The merger rate density of BHNSs shows an opposite trend, reaching the maximum value for lower $\alpha$. Finally, the merger rate density for BBHs seems to indicate a bell-shaped dependence on $\alpha$.

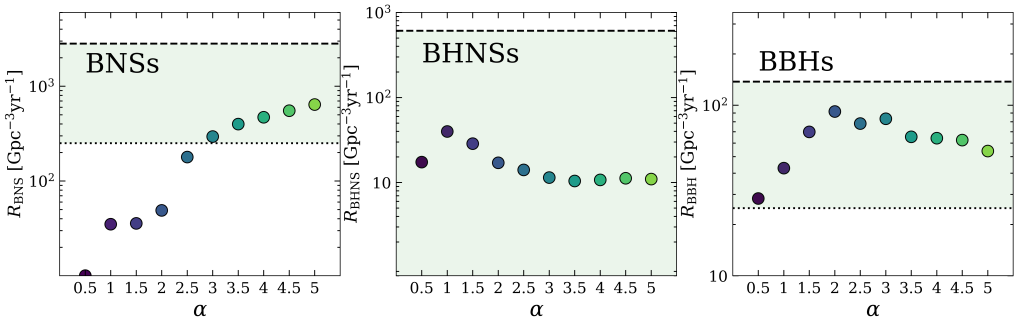


**Fig. 8.** Local merger rate density. Left, middle and right panel: local merger rate density of BBHs, BHNSs and BNSs, respectively. The green shaded region represent the 90 per cent credible interval of the merger rate density inferred by the LVC after O2, plus the BNS GW190425 (Abbott et al., 2019b,a, 2020b).

## 8. Conclusions

With MOBSE, the code I developed during my PhD, I performed in-depth studies of the demography of merging COBs. These studies were important i) to obtain a better grasp on the scenarios of the GW detections observed by the LVC, ii) to be ready for the astrophysical interpretation of the next GW events and iii) to develop astrophysical and statistical predictions for third-generation ground-based detectors.

On the one hand, my simulations show that only BHs with mass up to $\sim$ 40 – 45 $M_\odot$ merge via isolated binary evolution. On the other hand, I predict that BHs as massive as $\sim$ 65 $M_\odot$ can form from metal-poor single stars and loose binary systems. This prediction has a strong implication to distinguish between different formation channels of BBHs. The merger of BHs with mass > 45 $M_\odot$ would be a strong signature of dynamical formation (Bouffanais et al., 2019).

I also showed that the number of merging BBHs is very sensitive to progenitor's metallicity (higher at low $Z$). I found a similar trend for BHNSs, while the number of merging BNSs seem to be only mildly affected by progenitor's metallicity.

From my simulations it also emerges that the common-envelope phase is crucial for the formation of merging COBs. Indeed, thanks to the common-envelope phase, it is possible to shrink the orbital separation of systems that otherwise will not merge within a Hubble time. In particular, I found that high efficiency in ejecting the common envelope (high $\alpha$) boosts the number of merging BNSs. For BBHs and BHNSs the dependence on $\alpha$ is complicated by the fact that stellar radii for more massive stars are sensitive to metallicity.

I proposed a new prescription for the treatment of the natal kicks based on the idea that the strength of the natal kicks depends on the mass of the ejecta and the mass of the remnant. With this new approach, I was able to reproduce both the merger rate density inferred by the LVC and the natal kicks distribution of the observed Galactic pulsars.

Finally, I estimated the merger rate density by coupling my simulations with some prescriptions for the cosmological metallicity evolution and star formation rate.

*Acknowledgements.* I am grateful to M. Mapelli, my supervisor, for her illuminated guidance. I am indebted to M. Spera for his support as co-supervisor and friend. I also want to thank A. Ballone for the great discussions we had and the useful tips he gave me.

## References

Abbott B. P., et al., 2016, Phys. Rev. Lett., 116, 061102
Abbott B. P., et al., 2017, Phys. Rev. Lett., 119, 161101

Abbott B. P., et al., 2019a, Physical Review X, 9, 031040
Abbott B. P., et al., 2019b, ApJ, 882, L24
Abbott R., et al., 2020a, arXiv e-prints, p. arXiv:2010.14527
Abbott B. P., et al., 2020b, ApJ, 892, L3
Belczynski K., Bulik T., Fryer C. L., Ruiter A., Valsecchi F., Vink J. S., Hurley J. R., 2010, ApJ, 714, 1217
Belczynski K., et al., 2016, A&A, 594, A97
Bouffanais Y., Mapelli M., Gerosa D., Di Carlo U. N., Giacobbo N., Berti E., Baibhav V., 2019, ApJ, 886, 25
Burrows A., Hayes J., 1996, Phys. Rev. Lett., 76, 352
Chen Y., Bressan A., Girardi L., Marigo P., Kong X., Lanza A., 2015, MNRAS, 452, 1068
De Cia A., Ledoux C., Petitjean P., Savaglio S., 2018, A&A, 611, A76
Dessart L., Burrows A., Ott C. D., Livne E., Yoon S. C., Langer N., 2006, ApJ, 644, 1063
Fryer C. L., 1999, ApJ, 522, 413
Fryer C. L., Kusenko A., 2006, ApJS, 163, 335
Fryer C. L., Belczynski K., Wiktorowicz G., Dominik M., Kalogera V., Holz D. E., 2012, ApJ, 749, 91
Gessner A., Janka H.-T., 2018, ApJ, 865, 61
Giacobbo N., Mapelli M., 2018, MNRAS, 480, 2011
Giacobbo N., Mapelli M., 2019, MNRAS, 482, 2234
Giacobbo N., Mapelli M., 2020, ApJ, 891, 141
Giacobbo N., Mapelli M., Spera M., 2018, MNRAS, 474, 2959
Gräfener G., Hamann W. R., 2008, A&A, 482, 945
Gräfener G., Vink J. S., de Koter A., Langer N., 2011, A&A, 535, A56
Hall P. D., Tout C. A., 2014, MNRAS, 444, 3209
Hobbs G., Lorimer D. R., Lyne A. G., Kramer M., 2005, MNRAS, 360, 974
Hurley J. R., Tout C. A., Pols O. R., 2002, MNRAS, 329, 897
Iben Icko J., Livio M., 1993, PASP, 105, 1373
Ivanova N., et al., 2013, A&A Rev., 21, 59
Janka H.-T., 2017, ApJ, 837, 84
Janka H. T., Mueller E., 1994, A&A, 290, 496
Jones S., et al., 2013, ApJ, 772, 150
Kroupa P., 2001, MNRAS, 322, 231
Kusenko A., Mandal B. P., Mukherjee A., 2008, Phys. Rev. D, 77, 123009
Langer N., 2012, ARA&A, 50, 107
Madau P., Fragos T., 2017, ApJ, 840, 39
Mapelli M., Colpi M., Zampieri L., 2009, MNRAS, 395, L71
Moe M., Di Stefano R., 2017, ApJS, 230, 15
Nagakura H., Morinaga T., Kato C., Yamada S., 2019, ApJ, 886, 139
Sana H., et al., 2012, Science, 337, 444
Schwab J., Quataert E., Bildsten L., 2015, MNRAS, 453, 1910
Spera M., Mapelli M., 2017, MNRAS, 470, 4739
Spera M., Mapelli M., Bressan A., 2015, MNRAS, 451, 4086
Vink J. S., de Koter A., 2005, A&A, 442, 587
Vink J. S., de Koter A., Lamers H. J. G. L. M., 2001, A&A, 369, 574
Webbink R. F., 1984, ApJ, 277, 355
Woosley S. E., 2017, ApJ, 836, 244
Woosley S. E., 2019, ApJ, 878, 49
Woosley S. E., Pinto P. A., Martin P. G., Weaver T. A., 1987, ApJ, 318, 664